CHAOTIC AND QUASIPERIODIC MOTIONS OF THREE PLANAR CHARGED PARTICLES

Shu-Ming Chang*, Tai-Chia Lin†, Wen-Wei Lin‡

Abstract

We study two dynamical systems for the motion of three planar charged particles with charges $n_j \in \{\pm 1\}, j = 1,2,3$. Both dynamical systems are parametric with a parameter $\alpha \in [0,1]$ and have the same nonlinear terms. As $\alpha = 0,1$, the dynamical systems have no chaos. However, one dynamical system may create chaos as α varies from zero to one. This may provide an example to show that the homotopy deformation of dynamical systems cannot preserve the long-time dynamics even though the dynamical systems have the same nonlinear terms.

1 Introduction

In this paper, we study two dynamical systems of ordinary differential equations as follows.

$$\ddot{q}_j = (1-\alpha)\,\nabla_{q_j} W(q_1,q_2,q_3) \,+\, \alpha\,\dot{q}_j^{\perp}\,, \quad j=1,2,3\,, \tag{1.1}$$

and

$$(1-\alpha)\,\ddot{q}_j = \nabla_{q_j} W(q_1,q_2,q_3) \,+\, \alpha\, n_j\,\dot{q}_j^{\perp}\,, \quad j=1,2,3\,, \tag{1.2}$$

where $0 \le \alpha \le 1$ is a parameter, $q_j = q_j(t) = (q_{jx}(t), q_{jy}(t))\,, \ddot{q}_j = (\ddot{q}_{jx}, \ddot{q}_{jy})\,, \dot{q}_j^{\perp} = (-\dot{q}_{jy}, \dot{q}_{jx})$ and

$$W = \sum_{j\neq k}^{3} n_j n_k \,\log|q_j - q_k|\,. \tag{1.3}$$

*Department of Mathematics, National Tsing Hua University, Hsinchu, 30043, Taiwan, Email: m863254@am.nthu.edu.tw

†Department of Mathematics, National Chung Cheng University, Chiayi, 621, Taiwan, Email: tclin@math.ccu.edu.tw

‡Department of Mathematics, National Tsing Hua University, Hsinchu, 30043, Taiwan, Email: wwlin@am.nthu.edu.tw

Hereafter, $n_j \in \{\pm 1\}, j = 1,2,3$. The system (1.1) is a linear combination of two dynamical systems given by

$$\ddot{q}_j = \nabla_{q_j} W(q_1, q_2, q_3)\,, \quad j = 1,2,3\,, \tag{1.4}$$

and

$$\ddot{q}_j = \dot{q}_j^{\perp}\,, \quad j = 1,2,3\,. \tag{1.5}$$

As α varies from zero to one, the system (1.1) deforms (1.4) into (1.5). The system (1.2) is a linear combination of the system (1.4) and

$$-n_j\,\dot{q}_j^{\perp} = \nabla_{q_j} W(q_1, q_2, q_3)\,, \quad j = 1,2,3\,. \tag{1.6}$$

As α varies from zero to one, the system (1.2) deforms (1.4) into (1.6). Rescaling the time variable by $1/\sqrt{1-\alpha}$, the system (1.2) can be transformed into

$$\ddot{q}_j = \nabla_{q_j} W(q_1, q_2, q_3) \,+\, f_0\, n_j\, \dot{q}_j^{\perp}\,, \quad j = 1,2,3\,, \tag{1.7}$$

where $f_0 = \alpha/\sqrt{1-\alpha} \in [0, +\infty)$. Rescaling the time variable by $\sqrt{1-\alpha}$, we may transform (1.1) into

$$\ddot{q}_j = \nabla_{q_j} W(q_1, q_2, q_3) \,+\, f_0\, \dot{q}_j^{\perp}\,, \quad j = 1,2,3\,. \tag{1.8}$$

The system (1.7) and the system (1.8) have the same nonlinear terms. In particular, (1.7) is same as (1.8) if $n_1 = n_2 = n_3 = 1$.

We may rewrite the system (1.4) as follows.

$$\begin{cases} \ddot{q}_1 & = n_1\, n_2\, \dfrac{q_1 - q_2}{|q_1 - q_2|^2} + n_1\, n_3\, \dfrac{q_1 - q_3}{|q_1 - q_3|^2}\,, \\ \ddot{q}_2 & = n_2\, n_1\, \dfrac{q_2 - q_1}{|q_2 - q_1|^2} + n_2\, n_3\, \dfrac{q_2 - q_3}{|q_2 - q_3|^2}\,, \\ \ddot{q}_3 & = n_3\, n_1\, \dfrac{q_3 - q_1}{|q_3 - q_1|^2} + n_3\, n_2\, \dfrac{q_3 - q_2}{|q_3 - q_2|^2}\,. \end{cases} \tag{1.9}$$

Except the power of denominator, the system (1.9) is same as the planar charged three-body problem in the standard Coulomb's law, where n_j's play the role of charge. Therefore, we denote the system (1.4) as the planar "charged three-body" problem.

The system (1.4) comes from the dynamics of three quantized vortices in a nonlinear wave equation as follows.

$$\begin{cases} u_{tt} & = \Delta u + \frac{1}{\epsilon^2}(1 - |u|^2)u & \text{for } x \in \mathbb{R}^2\,, t > 0\,, \\ u|_{t=0} & = u_0(x) & \text{for } x \in \mathbb{R}^2\,, \\ u_t|_{t=0} & = u_1(x) & \text{for } x \in \mathbb{R}^2\,, \end{cases} \tag{1.10}$$

where $\epsilon > 0$ is a small parameter, u is a complex scalar field and the initial data u_0 has three vortex centers at $q_j(0), j = 1, 2, 3$, with winding numbers $n_j \in \{\pm 1\}, j = 1, 2, 3$. For the stability of the vortex structure in u, we require $n_j \in \{\pm 1\}, j = 1, 2, 3$. From particle and field theory [Dirac, 1938; Neu, 1990], we learned that planar charged particles with charges n_j's may be regarded as quantized vortices with winding numbers n_j's. Hereafter, we denote the charged particles at q_j's with charges n_j's as the quantized vortices with vortex centers q_j's and winding numbers n_j's. In Neu [1990], Neu investigated the planar electrodynamics by studying the dynamics of quantized vortices in (1.10). However, Neu's result is very complicated. As $\epsilon \to 0+$ and under a suitable time scaling, we derived the system (1.4) as simply asymptotic motion equations of quantized vortices in (1.10) (see e.g. Lin, [1999a] and Lin [1999]). Hence we may regard the system (1.4) as the interaction of planar charged particles at q_j's with charges n_j's.

The system (1.6) may come from the dynamics of three quantized vortices in a nonlinear Schrödinger equation as follows.

$$\begin{cases} -i\, u_t &= \Delta u + \frac{1}{\epsilon^2}(1 - |u|^2)u \qquad \text{for } x \in \mathbb{R}^2\,, t > 0\,, \\ u|_{t=0} &= u_0(x) \qquad \text{for } x \in \mathbb{R}^2\,, \end{cases} \tag{1.11}$$

where $\epsilon > 0$ is a small parameter, u is a complex scalar field and the initial data u_0 has three vortex centers at $q_j(0), j = 1, 2, 3$ with winding numbers $n_j \in \{\pm 1\}, j = 1, 2, 3$. For the stability of the vortex structure in u, we require $n_j \in \{\pm 1\}, j = 1, 2, 3$. The equation (1.11) is the Gross-Pitaevskii equation which is a well-known model on superfluids (cf. for example, Donnelly [1991], Frisch *et al.* [1992], Ginzburg & Pitaevskii [1958], Josserand & Pomeau [1995], Landau & Lifschitz [1989], and references of Nozieres & Pines [1990]). As $\epsilon \to 0+$ and under a suitable time scaling, the asymptotic motion equations of three vortices q_j's form the system (1.6) [E, 1994; Lin & Xin, preprint; Lin, submitted; Neu, 1990a].

The system (1.6) is the Kirchhoff problem which is a standard problem for the motion of quantized vortices (cf. p. 257 of Kirchoff [1883]). From Aref [1979, 1983], the Kirchhoff problem (1.6) is integrable. Hence the bounded and collisionless trajectories of the system (1.6) are either periodic or quasiperiodic. The system (1.4) describes the interaction of three planar charged particles which are denoted as three quantized vrotices. Our numerical results show that the bounded and collisionless trajectories of the system (1.4) are either periodic or quasiperiodic. By studying the system (1.2), we may understand the deformation of long-time dynamics from the planar "charged three-body" problem (1.4) to the Kirchhoff problem (1.6).

The system (1.8) is equivalent to the system (1.1). Moreover, the system (1.8) describes the motion of planar charged particles in an effect of the axial magnetic field as follows. In a small neighborhood of the charged particle at q_j with charge n_j, there is an axial magnetic field on the direction $(0, 0, n_j)$ with the strength f_0, respectively. Here $n_j \in \{\pm 1\}, j = 1, 2, 3$. Such an effect of the axial magnetic field can be found in the (Ginzburg-Landau) quantized vortices of a type II superconductor [de Gennes, 1989]. Note that we have regarded charged particles as quantized vortices.

The main purpose of this paper is to study the variety of long-time dynamics for (1.1) and (1.2) as α varies from zero to one. In this paper, we only consider collisionless orbits and investigate their long-time dynamics. All our results come from numerical experiments. We find an orbit $Q = \{(q_1, q_2, q_3)(t) | t > 0\}$ of (1.4) satisfying that Q is quasiperiodic if $n_1 = -n_2 = -n_3 = 1$, but Q is unbounded if $n_1 = n_2 = n_3 = 1$. For $\alpha \in [0, 1]$, let Q_α be the orbit of (1.1) such that $Q_0 = Q, Q_\alpha|_{\{t=0\}} = Q|_{\{t=0\}}$ and $\frac{d}{dt} Q_\alpha|_{\{t=0\}} = \frac{d}{dt} Q|_{\{t=0\}}$. As $n_1 = -n_2 = -n_3 = 1$, there exist two constants $0 < a_0 < a_1 < 1$ such that Q_α is chaotic for $\alpha \in (a_0, a_1)$ and quasiperiodic for $\alpha \in [0, a_0) \cup (a_1, 1]$. Furthermore, as $n_1 = n_2 = n_3 = 1$, there exist three constants $0 < a_0' < a_1' < a_2' < 1$ such that Q_α is bounded for $\alpha \in [a_0', 1]$, chaotic for $\alpha \in (a_1', a_2')$ and quasiperiodic for $\alpha \in [a_0', a_1') \cup (a_2', 1]$. Although Q_0 is quasiperiodic, the homotopy deformation (1.1) makes Q_α chaotic as $a_0 < \alpha < a_1, n_1 = -n_2 = -n_3 = 1$ or $a_1' < \alpha < a_2', n_1 = n_2 = n_3 = 1$. Hence the long-time dynamics of Q_α is not invariant as α varies from zero to one. This may provide an example to show that the homotopy deformation of dynamical systems cannot preserve the long-time $(t \to \infty)$ dynamics even though the dynamical systems have the same nonlinear terms. Note that from the standard theorems of ordinary differential equations, Q_α depends on α smoothly in any finite time interval as α varies from zero to one. For $\alpha \in [0, 1]$, let $\tilde{Q}_\alpha$ be the orbit of (1.2) such that $\tilde{Q}_0 = Q, \tilde{Q}_\alpha|_{\{t=0\}} = Q|_{\{t=0\}}$ and $\frac{d}{dt} \tilde{Q}_\alpha|_{\{t=0\}} = \frac{d}{dt} Q|_{\{t=0\}}$. As $n_1 = n_2 = n_3 = 1$, $\tilde{Q}_\alpha$'s have the same behavior as Q_α's when α varies from zero to one. As $n_1 = -n_2 = -n_3 = 1$, there exists $a_2 \in (0, 1)$ such that $\tilde{Q}_\alpha$ is quasiperiodic for $0 < \alpha < a_2$ but $\tilde{Q}_\alpha$ is unbounded for $\alpha > a_2$.

In the rest of this paper, we will provide our numerical evidences to show that the bounded and collisionless trajectories of the system (1.4) are either periodic or quasiperiodic in Section 2. Furthermore, we use the Newton's method to find a periodic orbit of the system (1.4) and we use the Poincaré section to obtain quasiperiodic orbits of the system (1.4). In Section 3 and 4, we show numerically the variety of long-time dynamics of Q_α's and $\tilde{Q}_\alpha$'s, respectively, as α varies from zero to one.

2 Numerical Results on the "Charged Three-Body" Problem

In this section, we present our numerical results on the "charged three-body" problem (1.4). Based on our numerical results, the bounded and collisionless trajectories of the system (1.4) are either periodic or quasiperiodic. For all ODE systems in this paper, we use the ODEABM predictor-corrector solver (see http://www.netlib.org/slatec) in FORTRAN 77 with the time step 0.05 sec on a Digital PW500au workstation with machine double precision eps $\approx 10^{-16}$.

Without loss of generality, we may consider $(n_1, n_2, n_3) = (1, 1, 1)$ and $(1, -1, -1)$ for the system (1.4). For the case $n_1 = n_2 = n_3 = 1$, the system (1.4) implies that q_j's repell each other and the collisionless orbits of (1.4) are unbounded. Now, we choose $n_1 = -n_2 = -n_3 = 1$ and we rewrite (1.4) as follows.

$$\begin{cases} \ddot{q}_1 &= -\dfrac{q_1 - q_2}{|q_1 - q_2|^2} - \dfrac{q_1 - q_3}{|q_1 - q_3|^2}\,, \\ \ddot{q}_2 &= -\dfrac{q_2 - q_1}{|q_2 - q_1|^2} + \dfrac{q_2 - q_3}{|q_2 - q_3|^2}\,, \\ \ddot{q}_3 &= -\dfrac{q_3 - q_1}{|q_3 - q_1|^2} + \dfrac{q_3 - q_2}{|q_3 - q_2|^2}\,. \end{cases} \tag{2.1}$$

2.1 Quasiperiodic Orbits of the System (2.1)

In this Section, we find collisionless and quasiperiodic orbits of the system (2.1). We simulate the solution of (2.1) with the initial conditions given by

$$\begin{aligned} &q_1^{(k)}(0) = (\xi_k, 1.7 + \eta_k), && \dot{q}_1(0) = (0,0)\,, \\ &q_2(0) = (-1, 0), && \dot{q}_2(0) = (0,0)\,, \\ &q_3(0) = (1, 0), && \dot{q}_3(0) = (0,0)\,, \end{aligned} \tag{2.2}$$

where the initial values of $q_1^{(k)}(0), k = 1, \cdots, 7$, varying in a half region of an ellipsoid E centered at $(0, 1.7)$, are denoted by "$*$" in Fig. 3.1. Here $\frac{1}{2}E = \{(x, y) : x \geq 0, \frac{x^2}{0.1^2} + \frac{(y-1.7)^2}{0.05^2} \leq 1\}$ is plotted by solid line in Fig. 3.1.

Fig. 3.1 is near here.

In Fig. 3.2 and 3.3, we plot the trajectories of q_j's and $\dot{q}_j$'s with different initial values $q_1^{(2)}(0) = (0, 1.7), q_1^{(5)}(0) = (0.05, 1.7)$ and $q_1^{(7)}(0) = (0.1, 1.7)$, respectively. For the other initial values $q_1^{(k)}(0), k = 1, 3, 4, 6$, the motion of q_j's is very similar to the motion of q_j's with initial values $q_1^{(k)}(0), k = 2, 5, 7$. Fig. 3.2 and 3.3 show that the system (2.1) numerically has a quasiperiodic solution as the initial value $q_1(0)$ in the region E.

Fig. 3.2 and 3.3 are near here.

In order to characterize the motion of q_j's, we compute (I) Poincaré maps, (II) Liapunov exponents and (III) spectrums of the waveforms, of the 12th order ODE system (2.1) with initial values given by (2.2). We describe our numerical computations on (I), (II) and (III) as follows.

(I) Poincaré maps: A Poincaré map program is written in FORTRAN according to the pseudo-code of Chap. 2 of Parker & Chua [1989]. The normal vector v_{11} of 11-dimensional hyperplane Σ_{11} is chosen by $v_{11} = g(x_\Sigma)$, where $x_\Sigma \in \Sigma_{11}$ and g is the vectorfield of (2.1). Let $\mathbb{P} : \Sigma_{11} \to \Sigma_{11}$ be the (first) Poincaré map. It is well known that if the points $\mathbb{P}^k(x_\Sigma), k = 1, 2, 3, \cdots$, densely fill out a closed curve, then the solution of (2.1) forms a quasi 2-periodic orbit i.e. two-torus. Otherwise, it is difficult to tell that the solution of (2.1) forms a quasi 2-periodic orbit (two-torus) or a quasi 3-periodic orbit (three-torus). For the identification of a quasi 3-periodic orbit, the second Poincaré map is necessary (cf. pp. 43-47 of Parker & Chua [1989]). The sampling of the second Poincaré maps uses a 10-dimensional hyperplane $\Sigma_{10} \subset \Sigma_{11}$ with a suitable normal vector. The points $\mathbb{P}^k(x_\Sigma)$'s that lie on Σ_{10} make up the orbit of the second Poincaré maps. In practice, none of the $\mathbb{P}^k(x_\Sigma)$'s lies exactly on Σ_{10}, so those $\mathbb{P}^k(x_\Sigma)$'s within $\epsilon \approx 10^{-5}$ of Σ_{10} are selected. Suppose that the orbit of the second Poincaré maps in Σ_{10} densely fills out a closed curve. Then the solution of (2.1) forms a quasi 3-periodic orbit i.e. three-torus. The extension to higher order Poincaré maps for quasi n-periodic orbits is obvious.

Fig. 3.4 is near here.

In Fig. 3.4(a)(b), the closed curves of the first (11-dimensional) Poincaré maps for the initial values of $q_1^{(1)}(0)$ and $q_1^{(3)}(0)$ are displayed, respectively. In Fig 3.5(a)-(d), the closed curves of the second (10-dimensional) Poincaré maps for the initial values of $q_1^{(4)}(0), \cdots, q_1^{(7)}(0)$ are plotted, respectively. Note that because of the use of ϵ-neighborhood, the closed curves here are somewhat fuzzy. Consequently, we observe that the solution of (2.1) forms a numerically quasi 2-periodic orbit if the initial value $q_1^{(k)}(0)$ is on y-axis and $|q_1^{(k)}(0)|$ is between 1.65 and 1.75. Moreover, the solution of (2.1) forms a numerically quasi 3-periodic orbit if the initial value $q_1^{(k)}(0)$ is on the open ellipsoid E but not on y-axis.

Fig. 3.5 is near here.

When the initial values $q_1^{(k)}(0)$'s in (2.2) are outside the region constrained by the dotted-line in Fig. 3.1, our numerical experiments show that the collision happens. Moreover, the orbit of the second Poincaré maps is shown in Fig. 3.6(a)-(c) if the initial value $q_1^{(k)}(0)$ is one of $q_1^{(8)}(0), q_1^{(9)}(0)$ and $q_1^{(10)}(0)$ denoted by "+" in Fig. 3.1, respectively. Here we observe that each orbit of the second Poincaré maps is broken and can not form a closed curve clearly.

(II) Liapunov exponents: Let $m_1(t), \cdots, m_n(t)$ be the eigenvalues of $\Phi_t(x_0)$ which is the transition matrix with $\Phi_0(x_0) = I_n$. The Liapunov exponents of x_0 are

$$\lambda_i = \lim_{t\to\infty} \frac{1}{t} |m_i(t)|, \quad i = 1, \cdots, n, \tag{2.3}$$

Fig. 3.6 is near here.

whenever the limit exists. A practical algorithm is developed here in FORTRAN 77 according to the pseudo-code of Chap. 3 of Parker & Chua [1989]. Liapunov exponents are a generalization of the eigenvalues at an equilibrium point of characteristic multipliers. They can be used to determine the stability of quasi-periodic and chaotic behavior as well as that of equilibrium points and periodic solutions.

We run our algorithm to compute the Liapunov exponents until the total time steps $= 2 \times 10^5$ with the initial conditions $q_1^{(k)}(0), k = 1, \cdots, 7$ in (2.2). For each k, the Liapunov exponents $\lambda_i^{(k)}, i = 1, \cdots, 12$ are located as follows.

$$-10^{-4} < \lambda_{12}^{(k)} \leq \cdots \leq \lambda_7^{(k)} < -10^{-6} < 10^{-6} < \lambda_6^{(k)} \leq \cdots \leq \lambda_1^{(k)} < 10^{-4}. \tag{2.4}$$

The numerical experiments show that for each k, the absolute values $|\lambda_i^{(k)}|, i = 1, \cdots, 12$ decrease about 1/10 provided the total time steps increase by a factor of 10. These indicate that the quasi 2- or 3-periodic solutions of (2.1) with initial conditions on E are stable but not asymptotic stable, i.e. the dimension of the attractor is zero.

(III) Spectrum of the waveform: The spectrum of the waveform $q(t) \equiv (q_1(t), q_2(t), q_3(t))$ with initial values $q_1^{(k)}(0), k = 3, 6, 7$ are computed by FFT subroutine by MATLAB and the frequency versus $\log_{10}(|fft(q)|_2)$ are displayed in Fig. 3.7(a)-(c), respectively. The spectrum distributions show that each solution with the associated initial value of $q_1^{(k)}(0)$'s on E is numerically quasi-periodic.

Fig. 3.7 is near here.

Numerical evidences of (I),(II) and (III) show that the collisionless trajectories of the "charged three-body" problem (2.1) can only occur a quasi 2- or 3-periodic orbit. In the rest of this section, we will find a periodic orbit of the system (2.1) by numerical simulation.

2.2 Periodic Orbit of the System (2.1)

Finding a periodic orbit is a fundamental problem on dynamical systems. In the standard charged three-body problem, the McGehee transform [McGehee, 1974] is useful to prove the existence of periodic orbits. By the McGehee transform, the collision manifold [Devaney, 1981] is bounded and it encloses a bounded region. Then the existence of periodic orbits is proved by the argument in Atela [1988]. Until now, there is no rigorous proof on the existence of periodic orbits in the "charged three-body problem" (2.1). One difficulty of finding periodic orbit is that the collision manifold is unbounded and it cannot enclose a bounded region.

The other difficulty of finding periodic orbit is that the periodic orbit is locally unstable. For example, suppose the isosceles "charged three-body problem" has a periodic orbit (q_1, q_2, q_3) such that

$$\begin{cases} q_{1x} \equiv 0, & q_{1y}(t) = y(t)\,, \\ q_{2x}(t) = x(t), & q_{2y}(t) = z(t)\,, \\ q_{3x}(t) = -x(t), & q_{3y}(t) = z(t)\,. \end{cases} \tag{2.5}$$

with initial data

$$x(0) = x_0 > 0, \quad y(0) = y_0, \quad z(0) = z_0, \quad \dot{x}(0) = \dot{y}(0) = \dot{z}(0) = 0\,, \tag{2.6}$$

where $y_0 \neq z_0$. Note that (2.5) implies that q_2 and q_3 are symmetric with respect to y-axis, and q_1 lies on y-axis. Then the system (2.1) becomes

$$\begin{cases} \ddot{x} &= -\dfrac{x}{x^2 + (y-z)^2} + \dfrac{1}{2x}\,, \\ \ddot{y} &= -\dfrac{2(y-z)}{x^2 + (y-z)^2}\,, \\ \ddot{z} &= \dfrac{y-z}{x^2 + (y-z)^2}\,. \end{cases} \tag{2.7}$$

By the last two equations of (2.7) and initial data (2.6), we have $y + 2z = 2C_0\,, \forall t > 0\,,$ where $C_0 = \frac{1}{2}y_0 + z_0$. Moreover, we obtain that

$$\begin{cases} \ddot{x} &= -\dfrac{x}{x^2 + (\frac{3}{2}y - C_0)^2} + \dfrac{1}{2x}\,, \\ \ddot{y} &= -\dfrac{3y - 2C_0}{x^2 + (\frac{3}{2}y - C_0)^2}\,. \end{cases} \tag{2.8}$$

It is easy to check that there are one positive, one negative and two purely imaginary eigenvalues of the linearized system of (2.8) with respect to any periodic solution of (2.8). Hence the periodic solution of (2.8) is locally unstable i.e. the periodic orbit of the isosceles "charged three-body problem" is locally unstable. The instablility of the periodic orbit makes it impossible to find the periodic orbit by the direct computation of (2.1) numerically.

To obtain the periodic orbit of (2.1), we use the Poincaré map method which is a generalization of the nonautonomous shooting method. Moreover, we apply the Newton-Raphson algorithm to find the fixed points of the one-sided Poincaré map $P_+ : \Sigma_p \to \Sigma_p$ (cf. e.q. Chap. 5 of Parker & Chua [1989]). Let $q \equiv (q_{1x}, q_{1y}, \dot{q}_{1x}, \dot{q}_{1y}, \cdots, q_{3x}, q_{3y}, \dot{q}_{3x}, \dot{q}_{3y})^T$ be the vector form of variables of (2.1) represented in the first order system. Take $\vec{h}_p = (0, 1, 0, \cdots, 0)^T \in \mathbb{R}^{12}$ as the normal direction of the Poincaré section Σ_p through the point $q_p = (0, 0, 0, 0, 1, 0, \cdots, 0)^T \in \mathbb{R}^{12}$. Define $H(q) = P_+(q) - q$. Then to locate a periodic orbit of (2.1) is equivalent to find a zero of $H(q)$.

We take $\|q^{(k+1)} - q^{(k)}\| \leq 10^{-6}$ as the stop criterion for each two adjacent vector $\{q^{(k)}, q^{(k+1)}\}$ computed by the Poincaré map algorithm. According to our numerical experience, the algorithm starts with $q^{(0)} = (0, 1.691335, 0, 0, 1, 0, 0, 0, -1, 0, 0, 0)^T$ and the algorithm stops at $q^{(4)}$ with components

$$
\begin{aligned}
(q_{1x}^{(4)}, q_{1y}^{(4)}) &= (0.000, 4.245e-16), & (\dot{q}_{1x}^{(4)}, \dot{q}_{1y}^{(4)}) &= (0.000, 1.010), \\
(q_{2x}^{(4)}, q_{2y}^{(4)}) &= (1.119, 0.846), & (\dot{q}_{2x}^{(4)}, \dot{q}_{2y}^{(4)}) &= (0.147, -0.505), \\
(q_{3x}^{(4)}, q_{3y}^{(4)}) &= (-1.119, 0.846), & (\dot{q}_{3x}^{(4)}, \dot{q}_{3y}^{(4)}) &= (-0.147, -0.505)\,.
\end{aligned}
$$

We compute the minimal distance d_{min} between $q^{(0)}$ and the numerical orbit of (2.1) from $q^{(3)} \in \Sigma_p$ to $q^{(4)} \in \Sigma_p$. The numerical result shows that $d_{min} \simeq 10^{-4}$. Thus we can fairly say that there is a periodic orbit of (2.1) through a point p near $q^{(0)}$ with components

$$
\begin{aligned}
(p_{1x}, p_{1y}) &\simeq (0, 1.691335), & (\dot{p}_{1x}, \dot{p}_{1y}) &= (0, 0), \\
(p_{2x}, p_{2y}) &= (1, 0), & (\dot{p}_{2x}, \dot{p}_{2y}) &= (0, 0), \\
(p_{3x}, p_{3y}) &= (-1, 0), & (\dot{p}_{3x}, \dot{p}_{3y}) &= (0, 0)\,.
\end{aligned}
$$

3 Numerical Results of the System (1.1)

From Section 1, the system (1.1) can be transformed to the system (1.8) given by

$$
\begin{cases}
\ddot{q}_1 &= n_1 n_2 \dfrac{q_1 - q_2}{|q_1 - q_2|^2} + n_1 n_3 \dfrac{q_1 - q_3}{|q_1 - q_3|^2} + f_0\, \dot{q}_1^{\perp}\,, \\
\ddot{q}_2 &= n_2 n_1 \dfrac{q_2 - q_1}{|q_2 - q_1|^2} + n_2 n_3 \dfrac{q_2 - q_3}{|q_2 - q_3|^2} + f_0\, \dot{q}_2^{\perp}\,, \\
\ddot{q}_3 &= n_3 n_1 \dfrac{q_3 - q_1}{|q_3 - q_1|^2} + n_3 n_2 \dfrac{q_3 - q_2}{|q_3 - q_2|^2} + f_0\, \dot{q}_3^{\perp}\,,
\end{cases}
\tag{3.1}
$$

where $f_0 = \alpha/\sqrt{1-\alpha} \in [0\,, +\infty)$. Now we focus on the ODE system (3.1) with $f_0 > 0$ and consider the cases $n_1 = 1, n_2 = n_3 = -1$ as well as $n_1 = n_2 = n_3 = 1$. We fix the initial conditions: $q_1(0) = (0, 1.7), q_2(0) = (-1, 0), q_3(0) = (1, 0), \dot{q}_j(0) = (0, 0), j = 1, 2, 3$ and vary the constant f_0 from 0 to 2.0.

Case 1: $n_1 = 1, n_2 = n_3 = -1$.

For the convenience of computations, we set $f_0 = 0.01, 0.1, 1.0$ and 2.0, respectively. In Fig. 3.8, we plot the trajectories of q_j's as $f_0 = 0.01, 0.1, 1.0$ and 2.0, where (q_1, q_2, q_3) is the solution of the system (3.1). The trajectories of q_j's are bounded and collisionless. They have a dancing pattern (changing partners) described as follows. Firstly, q_1 and q_3 rotate each other and move together but q_2 moves away from q_1 and q_3 in the time interval-1. Then q_2 comes forwards and attracts q_1 such that q_1 and q_2 rotate each other and move together. In addition, q_2 repelles q_3 such that q_3 moves away from q_1 and q_2 in the time interval-2. As time increases, the motion continues without collision and the motion style changes alternatively in different time intervals.

Fig. 3.8 is near here.

To study the dancing pattern of q_j's, we design a step function vs time interval by

$$\Gamma(t) = \begin{cases} ② & \text{if } |q_1(t) - q_2(t)| \leq |q_1(t) - q_3(t)|\,, \\ ③ & \text{if } |q_1(t) - q_2(t)| > |q_1(t) - q_3(t)|\,, \end{cases} \tag{3.2}$$

In Fig. 3.9(a)-(d), we plot the the step function Γ vs the specified time intervals for the cases $f_0 = 0.01, 0.1, 1.0$ and 2.0, respectively. Fig. (a), (d) show that the time period of q_1 rotating with q_2 and the time period of q_1 rotating with q_3 are almost same. However, Fig (b), (c) show that the time period of q_1 rotating with q_2 and the time period of q_1 rotating with q_3 are changed irregularly.

Fig. 3.9 is near here.

We now compute the Lyapunov exponents of the system (3.1) as f_0 varies from 0 to 2.5. Fig. 3.10(a)-(d) show that the system (3.1) is chaotic as $f_0 \in (0.0143, 1.68)$ but regular as $f_0 \in (0, 0.0143) \cup (1.68, 2.5)$. Actually, the numerical simulation becomes very vague and it is difficult to characterize when f_0 is close to the endpoints 0.0143 and 1.68.

Fig. 3.10 is near here.

We now compute the Poincaré maps of the system (3.1) with $f_0 = 0.01, 0.1, 1.0$ and 2.0, respectively. In Fig. 3.11(b)(c), we plot the first Poincaré maps (11-dim.) with $f_0 = 0.1$ projected onto $(q_{2y}, \dot{q}_{3x})$-plane and $f_0 = 1.0$ projected onto $(q_{2x}, \dot{q}_{3x})$-plane. The maps form a fractal pattern. Thus the trajectories of q_j's are fairly said to be chaotic as $f_0 = 0.1$ and 1.0. In Fig. 3.11 (a)(d), we plot the second Poincaré maps (10-dim.) of (3.1) with $f_0 = 0.01$ projected onto $(\dot{q}_{1y}, q_{3x})$-plane and $f_0 = 2.0$ projected onto $(\dot{q}_{1x}, q_{3y})$-plane. The maps form an invariant closed curve. Note that the fuzzy bands caused by using ϵ-neighborhood in computation. Thus the trajectories of q_j's are fairly said to be quasi 3-periodic as $f_0 = 0.01$ and 2.0. Furthermore, the spectrums of waveforms of (3.1) for $f_0 = 0.01, 0.1, 1.0$ and 2.0 are shown in Fig. 3.12.

Fig. 3.11 and 3.12 are near here.

All numerical evidences displayed here sustain our previous viewpoints that the system (3.1) has chaotic trajectories as $f_0 \in (0.0143, 1.68)$ and has quasi 3-periodic orbits as $f_0 \in (0, 0.0143) \cup (1.68, 2.5)$.

Remark: Suppose that the initial conditions are $q_1(0) = (0, 1.7), q_2(0) = (-1, 0), q_3(0) = (1, 0)$, and $\dot{q}_j(0) = (0.01, 0), j = 1, 2, 3$. Note that the initial velocities $\dot{q}_j(0)$'s are nonzero. Then by the same numerical methods, the motion of q_j's is chaotic if $f_0 \in (c, 1.4)$, where $c \approx 0.005$ and (q_1, q_2, q_3) is the solution of (3.1). Hence the nonzero initial velocities may change the interval of f_0 for the chaotic motion.

Case 2: $n_1 = n_2 = n_3 = 1$.

In this case, all q_j's repell each other and the collisionless orbits of (3.1) become unbounded as f_0 is close to zero. When we increase f_0, the trajectories of q_j's become bounded. In Fig. 3.13, we plot the diameters of q_j's as f_0 varies from e^{-2} to e^2.

Fig. 3.13 is near here.

Now we compute the largest Lyapunov exponents of (3.1) with f_0 from $e^{-0.5}$ to e^2 and plot them in Fig. 3.14. Numerical results show that the system (3.1) in this case is chaotic when f_0 is in a tiny interval $(1.268, 1.285)$. Otherwise, the system (3.1) has only quasi-periodic solutions.

Fig. 3.14 is near here.

As in Case 1, Fig. 3.15 plots the spectrums of waveforms as well as the first (11 dim.) and the second (10 dim.) Poincaré maps of (3.1), respectively, with (a) $f_0 = 1$, projected onto (q_{1x}, q_{2x})-plane; (b) $f_0 = 1.271$, projected onto (q_{1y}, q_{2x})-plane; (c) $f_0 = 5$, projected onto (q_{1x}, q_{2x})-plane. Here the second (10 dim.) Poincaré maps for the cases (a) and (c) form invariant closed curves. Thus the orbits can be regarded as quasi 3-periodic solutions. The first (11 dim.) Poincaré map for the case (b) forms a fractal pattern and the trajectory can be fairly said to be chaotic. All numerical evidences sustain our previous viewpoints.

Fig. 3.15 is near here.

4 Numerical Results of the System (1.2)

In this Section, we will study the long-time dynamics of (1.2). From Section 1, the system (1.2) can be transformed to the system (1.7) given by

$$\begin{cases} \ddot{q}_1 & = n_1\, n_2\, \dfrac{q_1 - q_2}{|q_1 - q_2|^2} + n_1\, n_3\, \dfrac{q_1 - q_3}{|q_1 - q_3|^2} + f_0\, n_1\, \dot{q}_1^{\perp}\,, \\ \ddot{q}_2 & = n_2\, n_1\, \dfrac{q_2 - q_1}{|q_2 - q_1|^2} + n_2\, n_3\, \dfrac{q_2 - q_3}{|q_2 - q_3|^2} + f_0\, n_2\, \dot{q}_2^{\perp}\,, \\ \ddot{q}_3 & = n_3\, n_1\, \dfrac{q_3 - q_1}{|q_3 - q_1|^2} + n_3\, n_2\, \dfrac{q_3 - q_2}{|q_3 - q_2|^2} + f_0\, n_3\, \dot{q}_3^{\perp}\,, \end{cases} \tag{4.1}$$

where $f_0 = \alpha/\sqrt{1-\alpha} \in [0\,, +\infty)$.

The system (4.1) can be regarded as a linear combination of the "charged three-body" problem and the Kirchhoff problem that is derived in Section 1. Note that if $n_1 = n_2 = n_3 = \pm 1$ the system (4.1) is equivalent to the Case 2 of (3.1) which has been discussed in Section 3. Now we focus on the system (4.1) with $n_1 = -n_2 = -n_3 = 1, f_0 > 0$ and the initial conditions: $q_1(0) = (0, 1.7), q_2(0) = (-1, 0), q_3(0) = (1, 0), \dot{q}_j(0) = (0, 0), j = 1, 2, 3$. From our numerical experiences, we observe that the system (4.1) has bounded solutions only when $0 \le f_0 \le f_0^* = 0.038$. For the case that $f_0 > f_0^*$, the trajectory of (4.1) becomes unbounded and is collisionless. Fig. 4.1 plots the diameters of the orbit range for (4.1) versus f_0 from e^{-5} to e^2.

Fig. 4.1 is near here.

As $f_0 > f_0^*$, the solution (q_1, q_2, q_3) of (4.1) behaves like that q_1, q_2 rotate each other and move toward infinity as t tends to infinity. In addition, q_3 forms a bounded orbit near $(-48, 0)$. Fig. 4.2 plots the unbounded orbit and the corresponding spectrum of waveform for the system (4.1) with

$f_0 = 0.5$. Here "*" and "o" denote the positions of $q_j, j = 1, 2, 3$ at $t = 550$ sec. and $t = 1000$ sec. respectively.

Fig. 4.2 is near here.

For $f_0 \in (0, 0.038)$, our numerical computations show that the orbits of (4.1) almost form quasi 3-periodic solutions which preserve the property of orbits as in the "charged three-body" problem (1.4). Fig. 4.3 plots the spectrum of waveform and the second (10 dim.) Poincaré map of (4.1) with $f_0 = 0.01$. We observe that the second Poincaré map forms an invariant closed curve projected onto $(\dot{q}_{1y}, \dot{q}_{2x})$-plane. This indicates that the orbit forms a quasi 3-periodic solution of (4.1).

Fig. 4.3 is near here.

Concluding Remarks:

We study two dynamical systems (1.1) and (1.2) with a parameter $\alpha \in [0, 1]$. The system (1.1) is a homotopy deformation from (1.4) the "charged three-body" problem to the system (1.5). The system (1.2) is also a homotopy deformation from (1.4) the "charged three-body" problem to (1.6) the Kirchhoff problem for three quantized vortices. As $\alpha = 0, 1$, the dynamical systems (1.1) and (1.2) have no chaos. However, one dynamical system may create chaos as α varies from zero to one. This may provide an example to show that the homotopy deformation of dynamical systems cannot preserve the long-time dynamics even though the dynamical systems have the same nonlinear terms.

Reference

Atela, P. [1988] "The charged isosceles 3-body problem," *Contemporary Math.* **81**, 43-58.

Aref, H. [1979] "Motion of three vortices," *Phys. Fluids* **22**(3), 393-400.

Aref, H. [1983] "Integrable, chaotic, and turbulent vortex motion in two-dimensional flows," *Ann. Rev. Fluid Mech.* **15**, 345-389.

Devaney, R. [1981] "Singularities in classical mechanical systems," *Ergodic Theory and Dynamical Systems I*, (Birkhäuser, Boston), pp. 211-333.

Dirac, P. [1938] "Classical theory of radiating electrons," *Proc. Roy. Soc. A* **167**, 148.

Donnelly, R. J. [1991] "Quantized Vortices in Helium II," in *Cambridge Univ. Press* (Cambridge).

E, W. [1994] "Dynamics of vortices in Ginzburg-Landau theories with applications to superconductivity," *Physica D.* **77**, 383-404.

Frisch, T., Pomeau, Y. & Rica, S. [1992] "Transition to dissipation in a model of superflow," *Phys. Rev. Lett.* **69**, 1644-1647.

de Gennes, P. G. [1989] "Superconductivity of metals and alloys," (Addison-Wesley Pub. Com. INC.).

Ginzburg, V. L. & Pitaevskii, L. P. [1958] "On the theory of superfluidity, *Sov. Phys. JETP* **7**, 585.

Josserand, C. & Pomeau, Y. [1995] "Generation of vortices in a model superfluid He^4 by the KP instability," *Europhysics Letters* **30**, 43-48.

Kirchhoff, G. [1883] "Vorlesungen über mathematische Physik," *Leipzig: Teubner*, vol. 1, Chap. 20, 257.

Landau, L. D. & Lifschitz, E. M. [1989] "Fluid Mechanics," *Course of theoretical physics* **6**, 2nd edition, Pergamon press.

Lin, F. H. [1999a] "Vortex dynamics for the nonlinear wave equations," *Comm. Pure Appl. Math.*, Vol. LII, No. 6, 737-761.

Lin, F. H. & Xin, J. X. "On the incompressible fluid limit and the vortex motion law of the nonlinear Schrödinger equation," preprint.

Lin, T. C. [1999] "Vortices for the nonlinear wave equation," *Disc. Conti. Dynam. Syst.*, Vol. 5, No. 2, 391-398.

Lin, T. C. "Spectrum of the linearized operator for the Ginzburg-Landau equation and its applications," submitted.

McGehee, R. [1974] "Triple collision in the collinear three body problem," *Invent. Math*, **27**, 191-227.

Neu, J. C. [1990a] "Vortices in complex scalar fields," *Physica D.* **43**, 385-406.

Neu, J. C. [1990] "Vortex dynamics of the nonlinear wave equation," *Physica D.* **43**, 407-420.

Nozieres, P. & Pines, D. [1990] "The theory of quantum liquids," *Vol. II: superfluid bose liquids* (Addison-Wesley Publishing Co., Inc.).

Parker, T. S. & Chua, L. O. [1989] "Practical Numerical Algorithms for Chaotic Systems," (Springer-Verlag).

http://www.netlib.org/slatec.

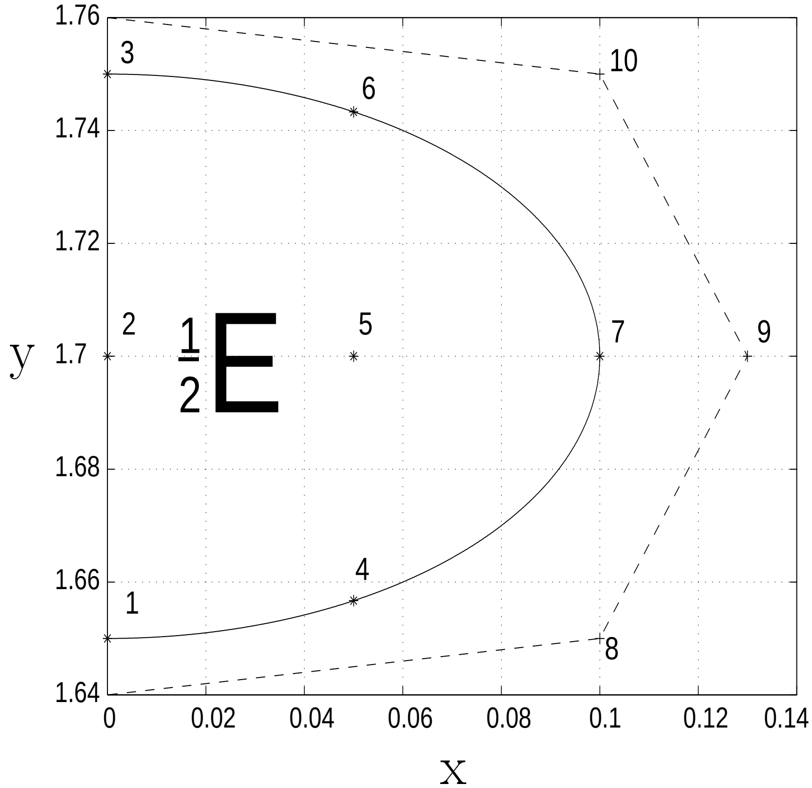

1.76
1.74
1.72
1.7
1.68
1.66
1.64
y
0
0.02
0.04
0.06
0.08
0.1
0.12
0.14
x
1
2
3
4
5
6
7
8
9
10
$\frac{1}{2}E$

Fig. 3.1.

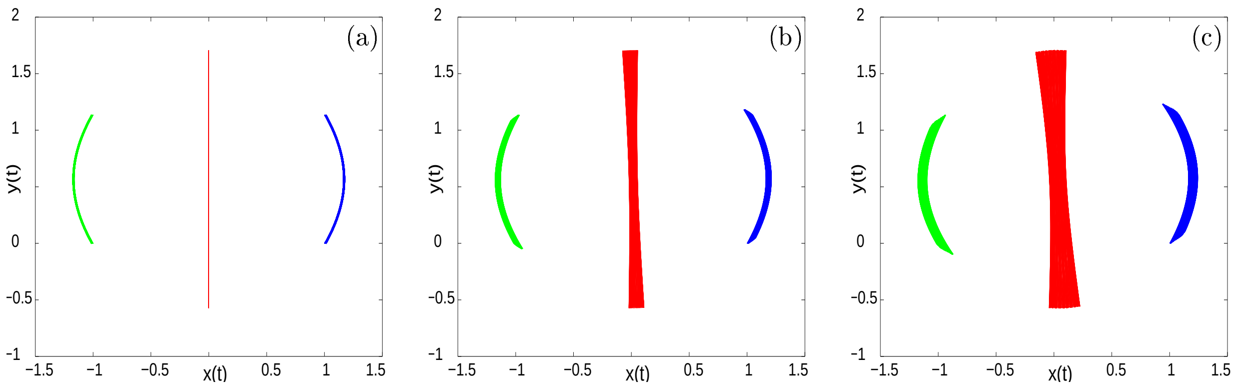

Fig. 3.2: Trajectory of positions of 3 vortices with (a) $q_1^{(2)}(0) = (0, 1.7)$; (b) $q_1^{(5)}(0) = (0.05, 1.7)$; (c) $q_1^{(7)}(0) = (0.1, 1.7)$.

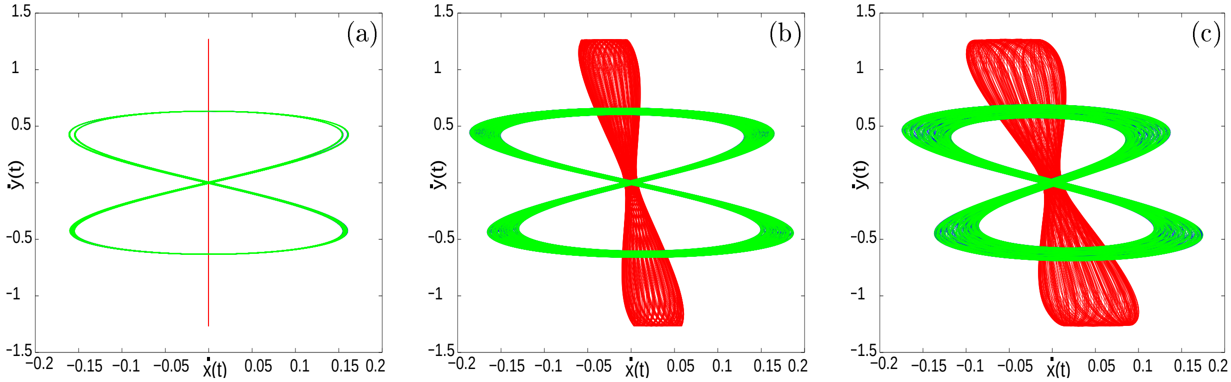

Fig. 3.3: Trajectory of velocity of 3 vortices with (a) $q_1^{(2)}(0) = (0, 1.7)$; (b) $q_1^{(5)}(0) = (0.05, 1.7)$; (c) $q_1^{(7)}(0) = (0.1, 1.7)$.

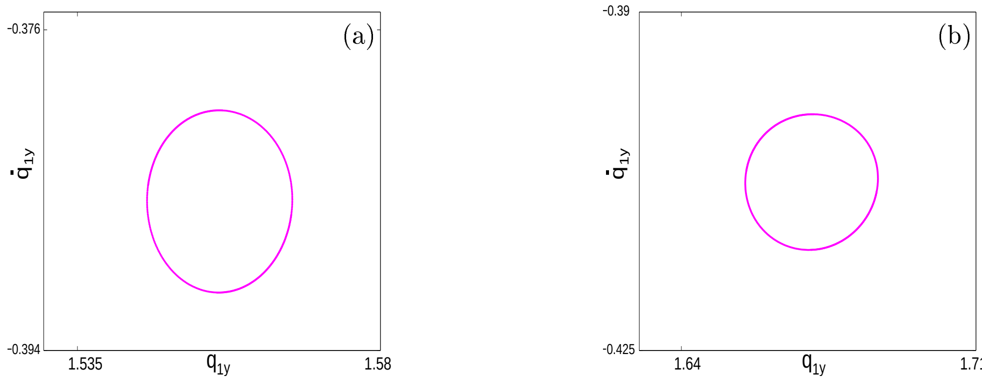

Fig. 3.4: First Poincaré maps (11-dim.) with (a) $q_1^{(0)}(0) = (0, 1.65)$ project onto $(q_{1y}, \dot{q}_{1y})$-plane; (b) $q_1^{(3)}(0) = (0, 1.75)$ project onto $(q_{1y}, \dot{q}_{1y})$-plane.

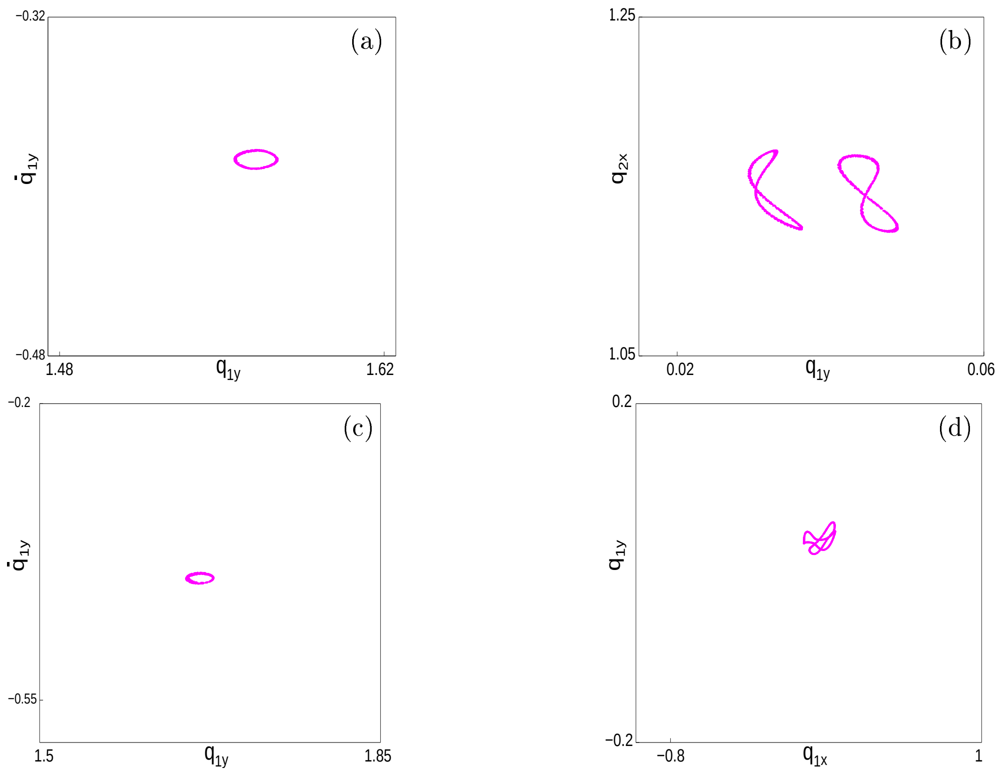

Fig. 3.5: Second Poincaré maps (10-dim.) with (a) $q_1^{(4)}(0) = (0.05, 1.6567)$ project onto $q_{1y}, \dot{q}_{1y}$-plane; (b) $q_1^{(5)}(0) = (0.05, 1.7)$ project onto (q_{1y}, q_{2x})-plane; (c) $q_1^{(6)}(0) = (0.05, 1.7433)$ project onto $(q_{1y}, \dot{q}_{1y})$-plane; (d) $q_1^{(7)}(0) = (0.1, 1.7)$ project onto (q_{1x}, q_{1y})-plane.

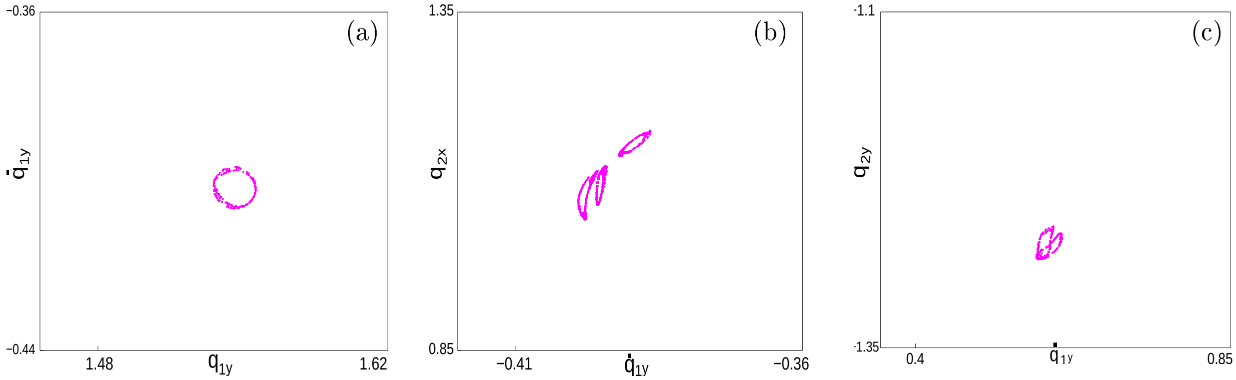

Fig. 3.6: Second Poincaré maps (10-dim.) with (a) $q_1^{(8)} = (0.1, 1.65)$ project onto $(q_{1y}, \dot{q}_{1y})$-plane; (b) $q_1^{(9)}(0) = (0.13, 1.7)$ project onto $(q_{1y}, \dot{q}_{2x})$-plane; (c) $q_1^{(10)}(0) = (0.1, 1.75)$ project onto $(\dot{q}_{1x}, q_{2y})$-plane.

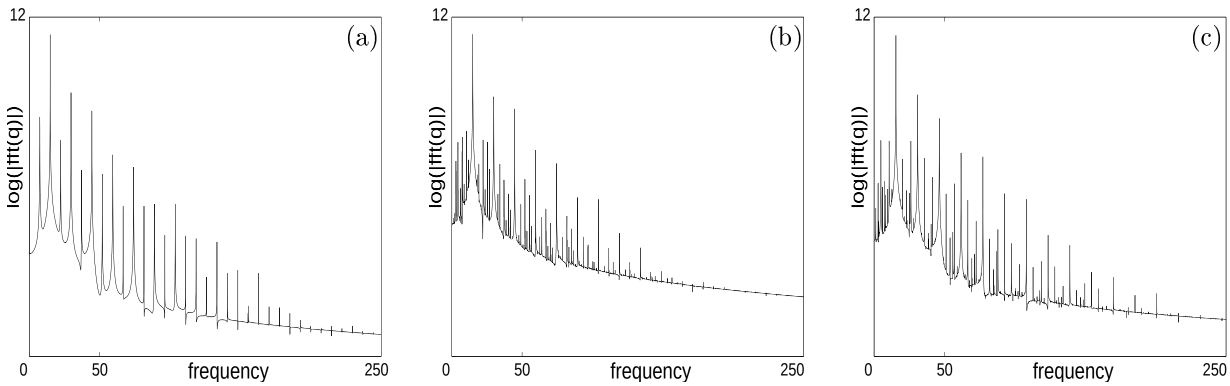

Fig. 3.7: The spectrum of the maveform $(q_1(t), q_2(t), q_3(t))$ with (a) $q_1^{(3)}(0) = (0, 1.75)$; (b) $q_1^{(6)}(0) = (0.05, 1.7433)$; (c) $q_1^{(7)}(0) = (0.1, 1.7)$.

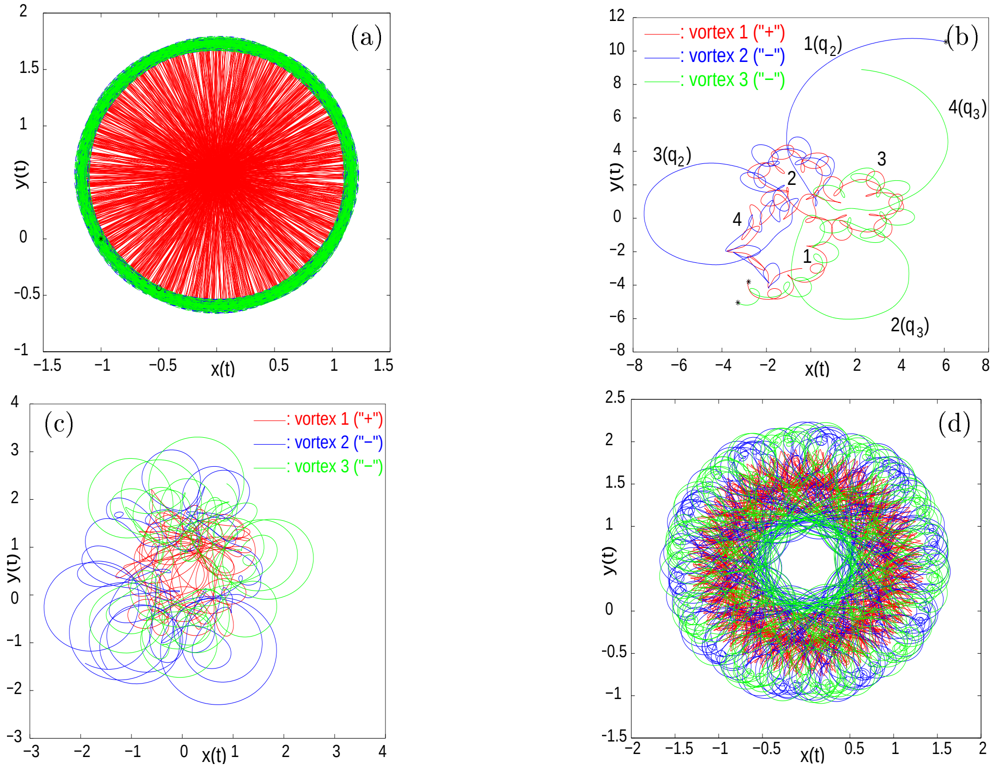

Fig. 3.8: The trajectories of q_j's in various time intervals (TI) with (a) $f_0 = 0.01$: $TI(0-150\text{ sec.})$ starting with $t_0 = 312230$ sec. (b) $f_0 = 0.1$: $TI_1(0-57\text{ sec.})$, $TI_2(57-58\text{ sec.})$, $TI_3(58-97\text{ sec.})$, $TI_4(97-116\text{ sec.})$ starting with $t_0 = 29250$ sec. (c) $f_0 = 1.0$: $TI(0-160\text{ sec.})$ starting with $t_0 = 51500$ sec. (d) $f_0 = 2.0$: $TI(0-80\text{ sec.})$ starting with $t_0 = 311800$ sec.

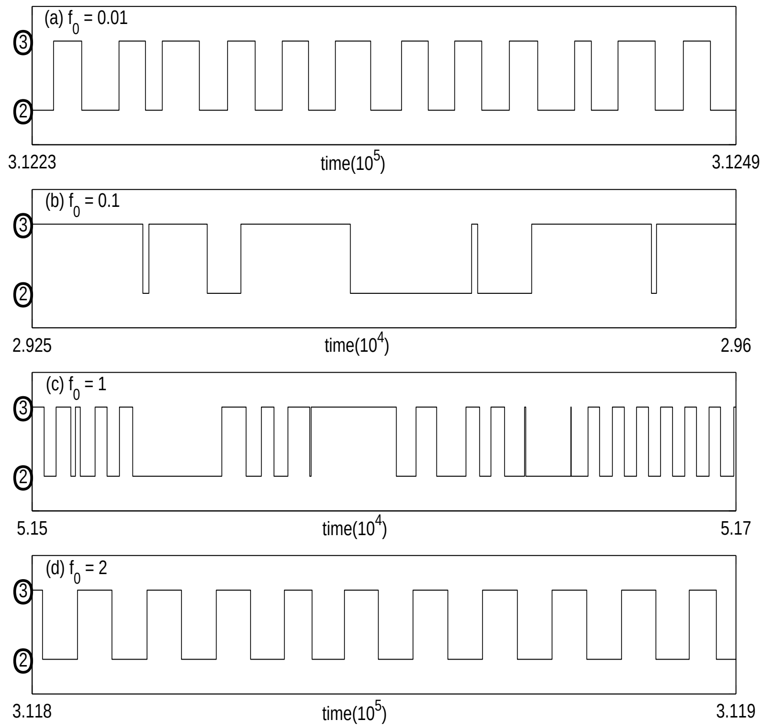

Fig. 3.9: The step function Γ defined in (3.2) vs the specified time intervals with (a) $f_0 = 0.01$: $3.1223(10^5) - 3.1249(10^5)$ sec. (b) $f_0 = 0.1$: $29250 - 29600$ sec. (c) $f_0 = 1.0$: $51500 - 51700$ sec. (d) $f_0 = 2.0$: $3.118(10^5) - 3.119(10^5)$ sec.

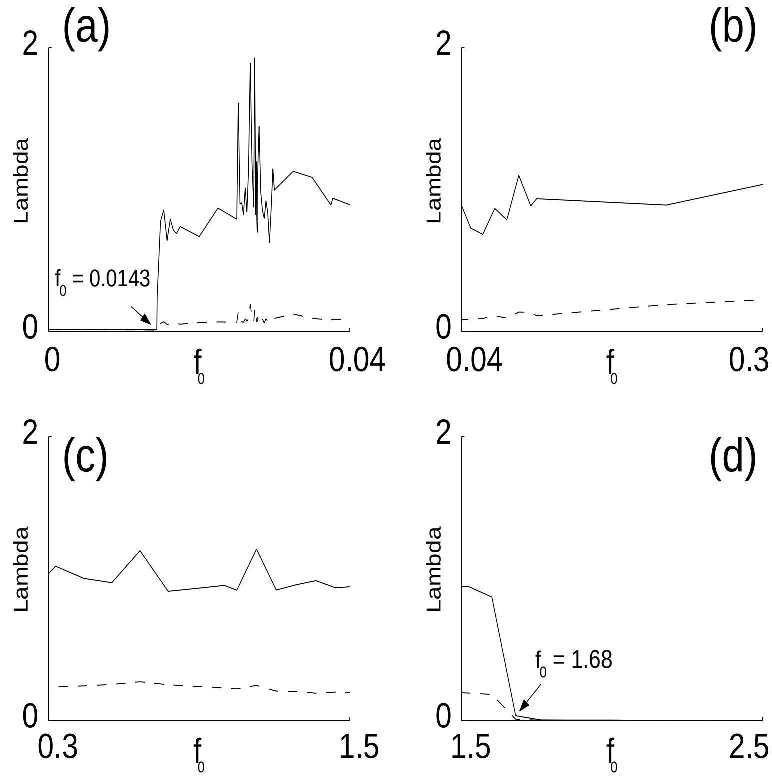

Fig. 3.10: The largest and the second largest Lyapunov exponents of the system (3.1) with (a) $f_0 \in (0, 0.04]$, (b) $f_0 \in [0.04, 0.3]$, (c) $f_0 \in [0.3, 1.5]$, (d) $f_0 \in [1.5, 2.5]$.

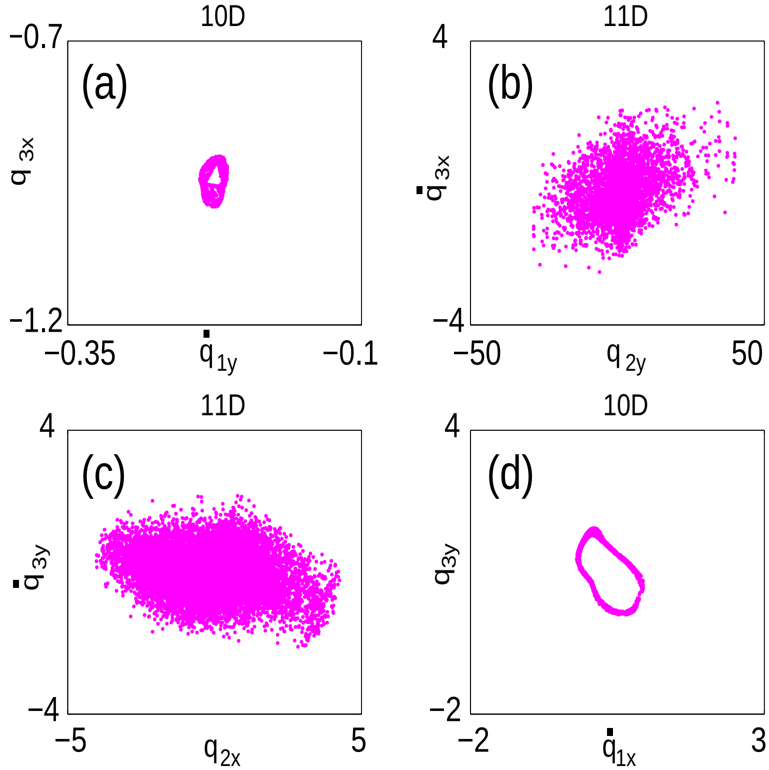

Fig. 3.11: Second Poincaré maps (10-dim.) with (a) $f_0 = 0.01$ onto $(\dot{q}_{1y}, q_{3x})$-plane; (d) $f_0 = 2.0$ onto $(\dot{q}_{1x}, q_{3y})$-plane; First Poincaré maps (11-dim.) with (b) $f_0 = 0.1$ onto $(q_{2y}, \dot{q}_{3x})$-plane; (c) $f_0 = 1.0$ onto $(q_{2x}, \dot{q}_{3x})$-plane.

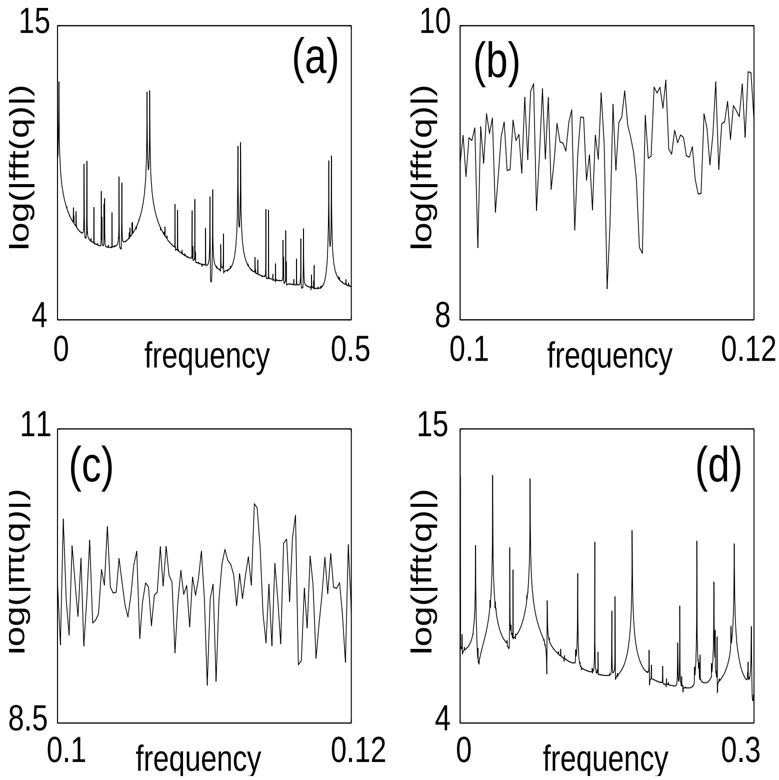

Fig. 3.12: The spectrum of the waveform of $(q_1(t), q_2(t), q_3(t))$ with (a) $f_0 = 0.01$; (b) $f_0 = 0.1$; (c) $f_0 = 1.0$; (d) $f_0 = 2.0$.

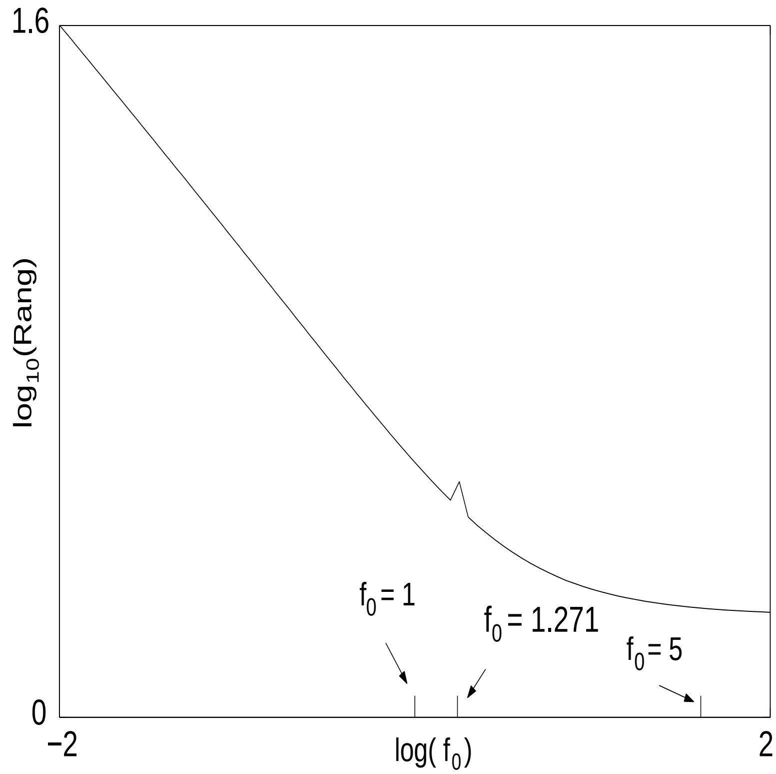

Fig. 3.13: Diameters of trajectories of (3.1) vs f_0 from e^{-2} to e^2.

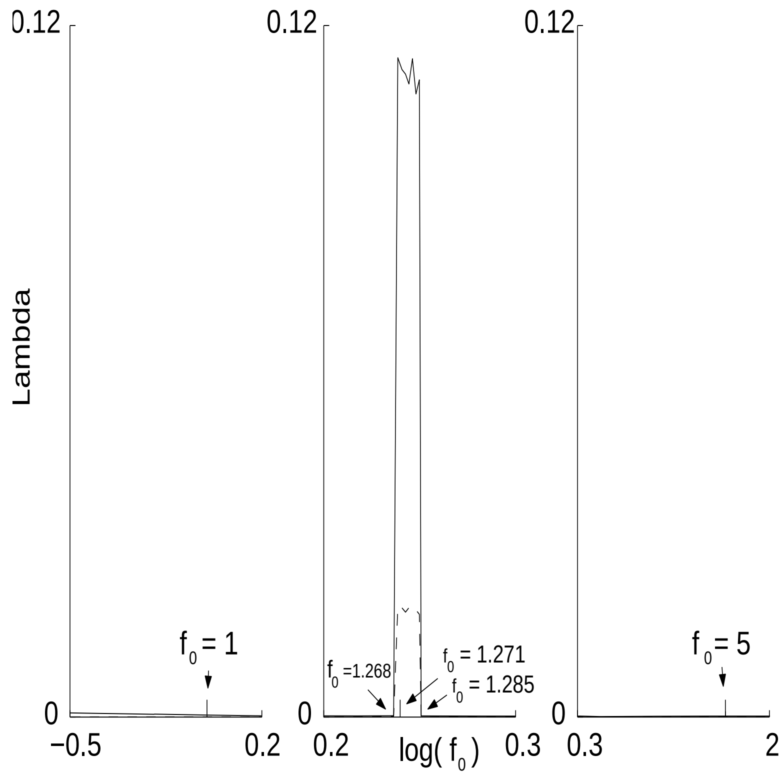

Fig. 3.14: The largest Lyapunov exponents of (3.1) vs f_0 from $e^{-0.5}$ to e^2.

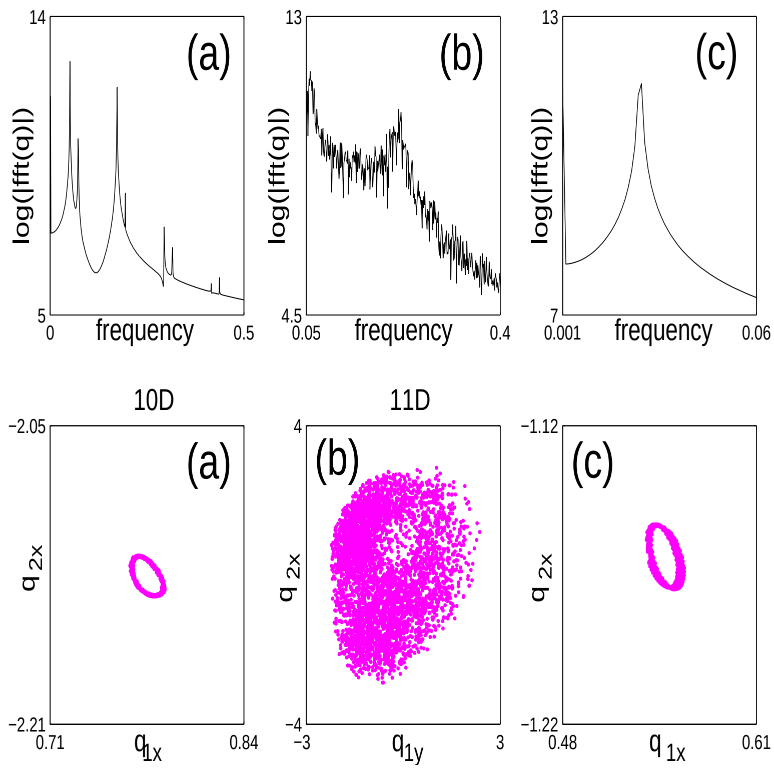

Fig. 3.15: The spectrums of waveforms as well as the first (11 dim.) and the second (10 dim.) Poincaré maps of (3.1) with (a) $f_0 = 1$; (b) $f_0 = 1.271$; (c) $f_0 = 5$.

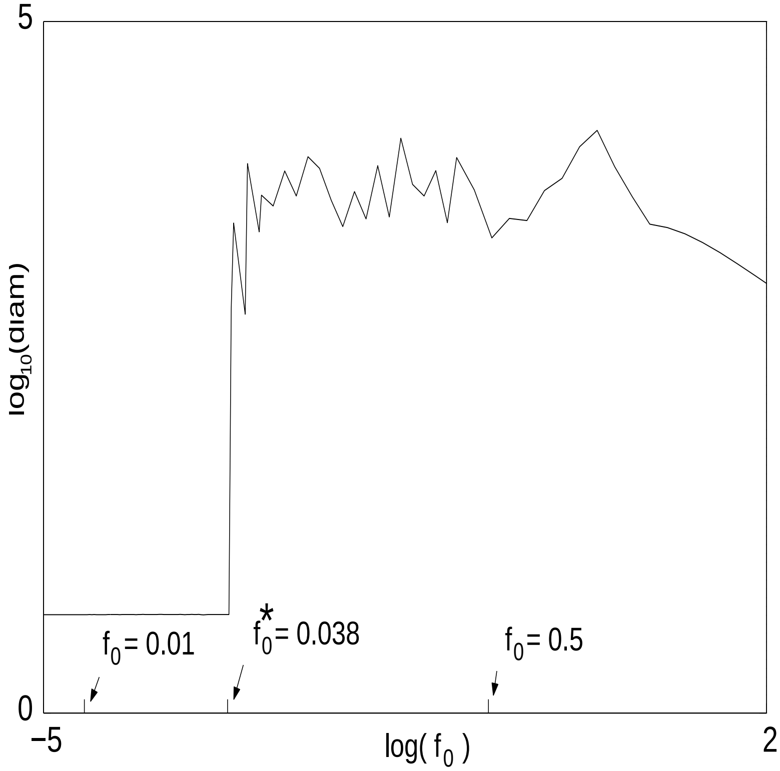

Fig. 4.1: Diameters of trajectories of (3.1) versus f_0 from e^{-5} to e^2

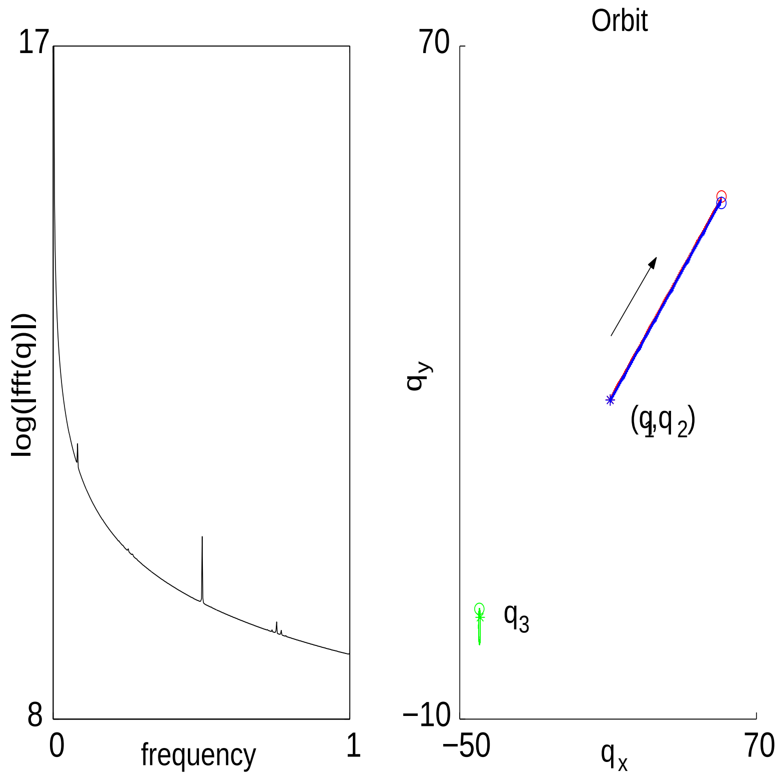

Fig. 4.2: Unbounded orbit (time: $550 - 1000$ sec.) and the spectrum of (4.1) with $f_0 = 0.5$.

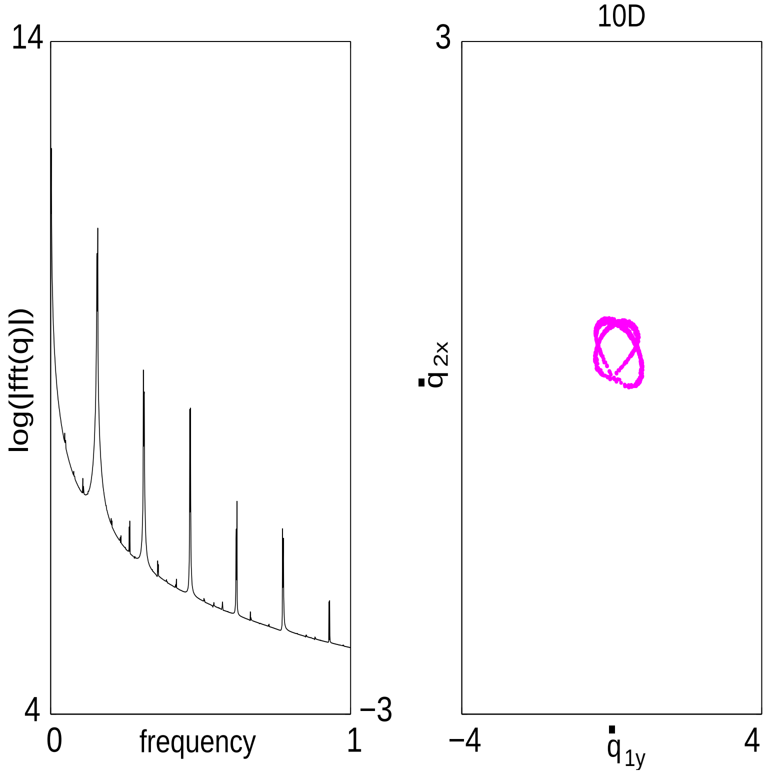

Fig. 4.3: The spectrum of waveform and the second (10 dim.) Poincaré map of (4.1) projected onto $(\dot{q}_{1y}, \dot{q}_{2x})$-plane with $f_0 = 0.01$.